Asem E. Metawa [1,2]

[1] Physics Department, Faculty of Science, Al-Baha University, SAUDI ARABIA
[2] Physics Department, Faculty of Science, Al-Azhar University, Cairo 11751, EGYPT

Investigation of Positive Ion Motion in Ar-N_2 RF Plasma Using a Cylindrical Langmuir Probe

This study presents a comparison of the Orbital Motion Limited (OML) and Allen-Boyd-Reynolds (ABR) models for describing positive ions behavior in low-temperature RF magnetron (Ar-N_2) plasma containing 70%, 60%, and 50% Ar in generated using 20W RF magnetron sputtering. Analysis performed on the I-V characteristics (0 to -40 V) obtained from a cylindrical Langmuir probe employed four criteria: a comparison of experimental and theoretical ion saturation current, the Sonin plot analysis, I^2-V the linearity in the ion saturation region, and the Pilling-Carnegie criterion ($d(\log_{10}V)/d(\log_{10}I)$) versus V- V_{plasma}. The ABR model accurately predicted the experimental results for the first and second criteria. The OML model agreed with the third and fourth criteria. Although this agreement was limited for the fourth criterion at β=0.16, the third criterion revealed increased linearity of the I^2-V curve of Ar-N_2 plasma with 70%, 60% Ar, indicating better agreement with the OML model in the saturation region than the 50% Ar plasma. Fourth criterion (the Pilling-Carnegie) indicates good agreement with the OML model for β=0.08 and 0.1, but deviation occurs at β=0.16.

***Keywords*:** Cylindrical Langmuir probe; Sonin plot; RF plasma; OML and ABR models
Received: 27 April 2025; **Revised:** 17 June 2025; **Accepted:** 23 June 2025

1. Introduction

Langmuir probes are essential tools for plasma diagnostics, particularly in determining the plasma parameters within the ion saturation region of the I-V characteristic [1]. Accurate measurements of positive ion current are crucial for understanding fundamental plasma physics and various plasma-enhanced surface processes, including chemical vapor deposition, ion implantation, etching, surface coating, and thin film fabrication [2-17]. The collection of positive ions by the probe is significantly influenced by their thermal motion and, in many cases, ion-neutral collision. Two primary theoretical models describe these processes: the orbital motion limited (OML) theory, applicable in the thick sheath limit the probe radius (r_p) is less than the Debye length ($r_p/\lambda_D \gg 1$), the Allen-Boyd-Reynolds (ABR) theory is suitable for the thin sheath limit the probe radius (r_p) is much larger than the Debye length ($r_p/\lambda_D \gg 1$) [18-21]. The OML model assumes the ions follow orbital trajectories, not all of which intersect the probe, while the ABR model assumes radial trajectories, leading to complete ion collection [18,19]. However, the applicability of either model *a priori* is often uncertain, and experimental results frequently fall between their predictions [12,17]. Neither model fully accounts for ion-neutral collision [22,23], highlighting the need for a more comprehensive model incorporating these effects [24-26]. Furthermore, challenges arise in interpreting Langmuir probe data in RF plasma due to RF pick up and neutral collisions, especially in high-density plasma where deviation from theoretical predictions occurs [27-29].

This study addresses these challenges by experimentally investigating positive ion collection in low-temperature RF argon–nitrogen plasma using a cylindrical Langmuir probe. The applicability of OML and ABR models was evaluated by analyzing the ion saturation region of the I-V curve characteristics using four criteria: (1) a comparison with theoretical predictions, (2) the Sonin plot analysis, (3) I^2-V linearity, and (4) the Pilling-Carnegie criterion ($d(\log_{10}V)/d(\log_{10}I)$) versus V-$V_{plasma}$. The experimental setup and theoretical framework, including relevant model equations (Poisson's equation and the ion continuity equation), are described in the following section. The selection of an appropriate theoretical model for plasma diagnostics remains uncertain prior to its application. Various approaches exist for modeling gas discharges, including analytical models, fluid models, the Boltzmann transport equation, Monte Carlo (MC) simulations, Particle-in-Cell Monte Carlo Collisions (PIC-MCC) simulations, and hybrid models combining fluid and Monte Carlo methods [30-35]. Each approach has unique advantages and limitations, with the optimal choice dependent on specific gas discharge and conditions.

2. Experimental Part

This section details the experimental setup used to diagnose an RF plasma generated by a magnetron sputtering system (schematic shown in Fig. 1a) [8]. The system comprised a cylindrical silica glass chamber (24 cm inner diameter and 20 cm length) evacuated to get a base pressure of 5×10^{-6} mbar. The vacuum system consists of an Edward 5 rotary pump and silicon oil diffusion. The gas mixture ratio was controlled by independently regulating the flow rate of Ar and N_2 gases using flow meter control (Tylan General). The base pressure was 5×10^{-6} mbar. For a

50/50 Ar/N_2 mixture, the resulting partial pressures were 2.5×10^{-3} mbar for Ar and 2.5×10^{-3} mbar for N_2. For a 60/40 Ar/N_2 mixture, partial pressures were adjusted to 3×10^{-3} mbar for Ar and 2×10^{-3} mbar for N_2. The 70/30 Ar/N_2 mixture results in partial pressures 3.5×10^{-3} mbar for Ar and 1×10^{-3} mbar for N_2, resulting in a total of $5\text{x}10^{-3}$ mbar (measuring using a manometer). The gas flow rate was regulated using flow meters (Tylan General). A 6 cm diameter steel magnetron gun connected to a matching network and a 13.5 MHz RF power supply operating at 20 W. A matching circuit is essential for delivering maximum forward power to the plasma chamber while minimizing reflected power to the RF system. The cylindrical Langmuir probe is immersed between the target and substrate. The space between the substrate and the target was held at 5 cm.

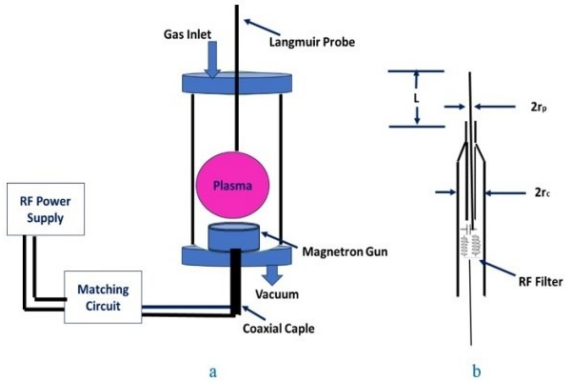

Fig. (1) A schematic diagram of the RF plasma magnetron sputtering system and Langmuir probe system

Accurate Langmuir probe measurements in RF plasma require careful consideration of several electrical and electronic arrangements, such as probe size, probe material, RF filter, and proper grounding. Figure (1b) illustrates a cylindrical Langmuir probe design. A 3 mm long cylindrical molybdenum wire (a radius r_p of 0.35 mm) was chosen to minimize secondary electron emission and sputtering processes resulting from collisions between particles and the probe. The probe electric circuit included a 100 V_{DC} power supply and a 100 kΩ, 10-turn potentiometer for precise voltage control. An RF filter (two 75 μH inductors and a 100 nF capacitor) was connected to the single probe to block RF interference, ensuring only DC was measured. Optimal probe design requires careful choices of r_p, r_c, and L (probe radius, chamber radius, and probe length, respectively) to satisfy the following conditions: $r_p, r_c \ll L$, $\lambda_D \ll L$, and $L \ll \lambda_e$, where λ_e is the mean free path of electrons and λ_D is the Debye length. These conditions ensure accurate sheath measurements.

3. Results and Discussion

Several criteria exist for analyzing the results of ions collected by a cylindrical Langmuir probe. These criteria differ significantly in critical aspects and are discussed in this work. The OML or radial nature of the collected positive ions is independent of the chosen criterion. The following section describes these criteria.

The first criterion compares the experimental results of the I-V probe curve characteristics obtained at negative probe bias (within the ion sheath) to the theoretical predictions based on the radial model and OML theory. The governing equations for each model are given below [36]:

$$I_e = I_{es}\, exp[\frac{e(V-V_{plasma})}{k_B T_e}] \quad (1)$$

The electron saturation current, I_{es} is given by

$$I_{es} = eAn_e(\frac{k_B T_e}{2\pi m_+}) \quad (2)$$

where e is the electron charge, A is the cylindrical probe surface area, n_e is the electron density, T_e is the electron temperature, k_B is the Boltzmann constant, and m_+ is the ion mass

Figure (2) shows the experimental I-V characteristics curve of cylindrical probes in argon-nitrogen plasma and theoretical curves according to the radial and OML theories. The OML curve occurs at $V<V_{Floating}$, where V_{plasma} is the plasma potential, $V_{Floating}$ is the floating potential, and V is the probe potential. The radial curve is valid for potentials $V<V_{plasma}$, according to the following equation [36]:

$$V < V_{plasma} - (\frac{2k_B T_+}{e}) \quad (3)$$

Figures (2a), (2b), and (2c) show the I-V characteristics for an RF Ar-N_2 magnetron plasma at the RF power of 20 W and a pressure with varying the Ar concentration: (a) 70%, (b) 60%, and (c) 50 %. The experimental data in figures (2a) and (2b) show good agreement with the prediction from the radial model ABR across a wide range of positive ion current regions. However, figure (2c) shows less agreement with the ABR model. Significant discrepancies exist between the experimental curve and the OML model prediction. Therefore, the success of this criterion depends on the agreement between experimental results and either the radial or OML model.

The OML theory assumed that the orbital angular momentum of ions limits the ion current in the saturation region. At the sheath edge assumed the Maxwellian of ion energy distribution. The plasma potential $V_p(r)$ as a function of r, the radius of circular orbital motion around the probe.

The second criterion utilizes a Sonin plot [37], a suitable representation for the positive ion collection by the cylindrical Langmuir probe. This criterion plots the dimensionless ion current $I'(x_p, y_p, \beta)$ from Eq. (4) [38]

$$I'(x_p, y_p, \beta) = \frac{I_+(x_p, y_p, \beta)}{e r_p n_+}\sqrt{\frac{m_+}{2\pi k_B T_e}} \quad (4)$$

versus dimensionless parameters derived from the ion current and probe radius in Eq. (5). The probe

potential is held constant during the analysis in this criterion [38]:

$$I'(x_p, y_p, \beta) x x_p^2 = \frac{I_+(x_p, y_p, \beta) e r_p}{\varepsilon_0} \sqrt{\frac{m_+}{2\pi k_B^3 T_e^3}} \quad (5)$$

where ε_0, r, x_p, and I_+ are the vacuum dielectric permittivity constant, probe radius, dimensionless probe radius, and ion saturation current, respectively.

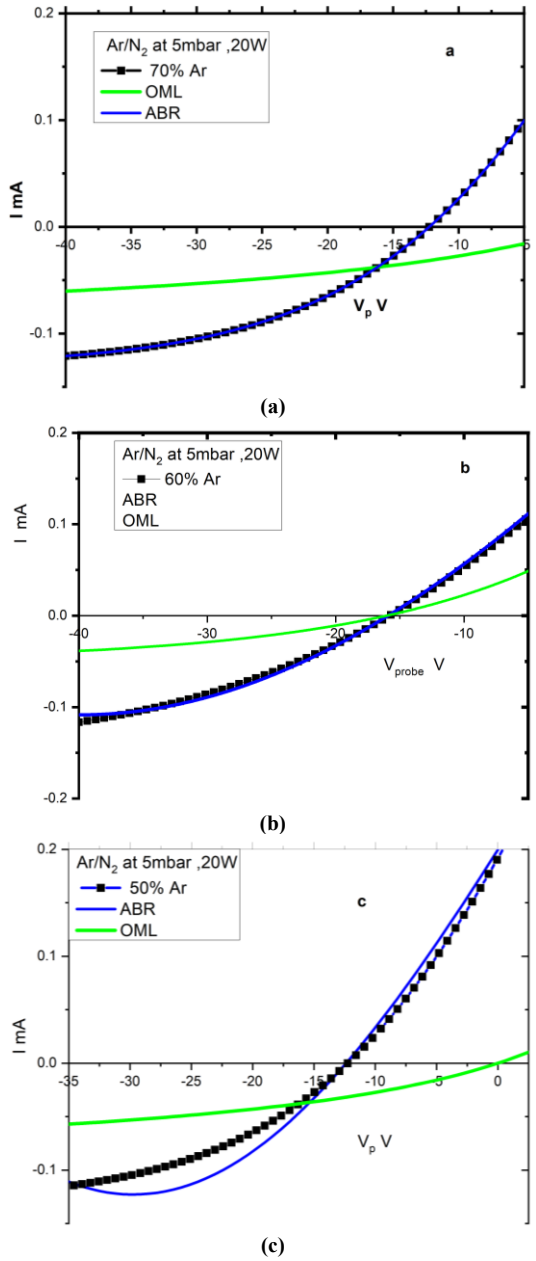

Fig. (2) The I-V characteristics in the ions saturation region of RF Ar-N_2 magnetron plasma at a pressure of 5x10^{-3} mbar and the power RF 20 W with varying the Ar concentration is varied as follows: (a) 70%, (b) 60%, and (c) 50%. Experimental results compare the orbital (green) and radial (blue) models

The dimensionless probe radius x_p and Debye length λ_D are defined as [39]:

$$x_p = \frac{\lambda_D}{r_p} \quad (6)$$

and

$$\lambda_D = \sqrt{\frac{\varepsilon_0 k_B T_e}{e n_e}} \quad (7)$$

The dimensionless probe biased potential y_{sp} can be calculated from equation [39]:

$$y_{sp} = -\frac{eV_{sp}}{k_B T_e} \quad (8)$$

where T_e is the electron temperature obtained from the integrated EEDF curve or the slope of the log current-voltage curve for a probe

The Sonin plot used to analyze the motion of the ions around the Langmuir probe depends on two key parameters: normalized thickness sheath, space potential y_{sp}, and the temperature ratio $\beta=T_+/T_e$ are the ion and electron temperatures, respectively. The OML predicts the Sonin plot coordinate from the equations [38]:

$$y_{sonin\ plot} = \frac{2}{\sqrt{\pi}} \sqrt{\beta + \frac{eV_{sp}}{k_B T_e}} \quad (9)$$

Plot versus

$$x_{sonin\ plot} = \frac{2}{\sqrt{\pi}} \sqrt{\beta + \frac{eV_{sp}}{k_B T_e}} \left(\frac{r_p}{\lambda_D}\right)^2 \quad (10)$$

The validity of different theoretical models is assessed by comparing the experimental Sonin plot to the theoretical prediction. These include the Sonin plot in (Sonin 1966) [38], the Laframboise OML model (with Peterson and Talbot's fitting curve) [38-40] and the Allen, Boyd, Renold ABR theory (radial model) at different values of β [41-43].

Figure (3) represents the experimental Sonin plot curve for positive ions in RF Ar-N_2 magnetron plasma collected by the cylindrical probe for y_{sp}=25 at values of β=0.08, 0.1, and 0.16. The experimental results suggest that the radial theory is the best description for collection in the Ar-N_2 plasma, while the OML theory is not consistent with the experimental observation.

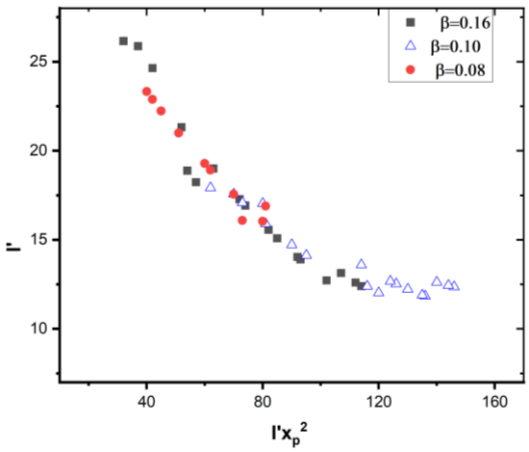

Fig. (3) The Sonin plot of positive ions collected by the cylindrical probe in RF Ar-N_2 magnetron plasma for y_{sp}=25 under values of β=0.08, 0.1, and 0.16

The third criterion analyzes the linearity of the relationship between the square of the ion current (I^2) and the negative probe potential (V) within the ion

saturation region of the experimental curve. The ion current is given by [22] for V<<<V_{plasma}:

$$I_+ = -eAn_+\sqrt{\frac{k_BT_+}{2\pi m_+}}\frac{2}{\sqrt{\pi}}\sqrt{(1-\frac{e\|V-V_{plasma}\|}{k_BT_+})} \quad (11)$$

where T_+ is the ion temperature

This criterion can determine ion density [3,28]. This criterion depends on the linearity of the I^2-V curve. The advantage of this criterion is that it can be used over a wide range of the current-voltage curve. This criterion determines whether the motion of positive ions around the probe is orbital or non-orbital. Figure (4) shows the I^2-V characteristic curves for argon-nitrogen plasma under different conditions.

Figures (4a) and (4b) depict the I^2-V curves of Ar-N_2 plasma with 70% and 60% Ar, respectively, exhibiting greater linearity in the ion saturation compared to the curve in Fig. (4c) at 50% Ar. This indicates that the linearity of the I^2-V curves in this region correlates with the Ar/N_2 gas mixture ratio, with higher Ar concentration associated with greater linearity. The increased linearity in figures (4a) and (4b) suggests better agreement with the OML theory in these cases, while the reduced linearity in Fig. (4c) indicates a deviation from the OML model. However, this correlation doesn't prove that the OML theory solely governs the observed motion of ions in RF Ar-N_2 plasma. Increase the Ar percentage, reduce charge-exchange collision affecting ion motion before the probe arrival [26]. The following criterion will help us to determine the best model to describe the observed ions' motion.

The fourth criterion, the Pilling-Carnegie criterion, assesses ion collection mechanisms by analyzing the relationship between $d(\log_{10}V)/d(\log_{10}I)$ and V-V_{plasma} [22,44]. According to this criterion, ion motion is consistent with the OML theory when the curve of $d(\log_{10}V)/d(\log_{10}I)$ versus V curve tends to the absolute 2 value. Figure (5) shows this relationship in the ion saturation region (V<<V_{plasma}) for β=0.08, 0.1, and 0.16. The curves β=0.08 and 0.1 approach the absolute 2 value, indicating the good agreement of the OML model. However, for β=0.16, the curve doesn't approach the absolute 2 value only over a limited voltage range. This suggests that the OML model provides a reasonable approximation for β =0.08 and 0.1, deviations occur at β=0.16 in an RF Ar-N_2 plasma.

Table (1) summarizes the applicability of the four criteria to RF Ar-N_2 plasma using a cylindrical Langmuir probe. The ABR model shows agreement with two criteria (comparison of experimental and theoretical I-V curves and Sonin plot), while the OML model shows agreement with two criteria (linearity of I^2-V and Pilling-Carnage) under specific conditions. Table 1 also details the Advantages and disadvantages of each criterion, considering both orbital and radial ion motion.

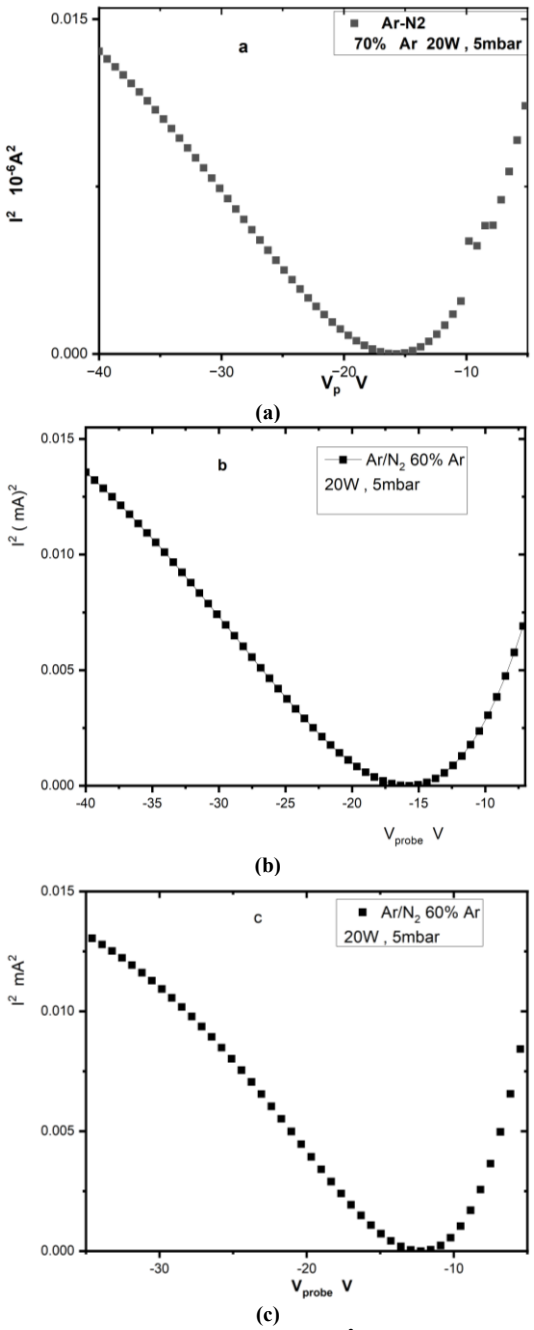

Fig. (4) Square ion saturation current I^2 plotted against probe voltage V for RF Ar-N_2 magnetron plasma at power source 20 W, and pressure 5mbar. The Ar concentration is varied as follows: (a) 70 % Ar,(b) 60 % Ar, and (c) 50 % Ar

The study highlights the limitations of the OML and ABR models in accurately predicting low-temperature RF magnetron sputtering Ar/N_2 plasma at low power, several challenges contribute to these limitations, including the effect of RF waves, magnetic field, and the electronegativity introduced by nitrogen molecules. Applying these models using the four criteria mentioned before may reveal significant deviations, particular with increase the N_2 percentage. This is evidenced in a comparison of experimental and theoretical ion saturation current criteria, a trend

supported by previous studies, the ABR, and OML in Ar plasma with the I-V curve [21-23]. The discrepancies underscore the need for a more comprehensive model. Particularly considering the motion of ions in nitrogen plasma, near the magnetic field at the target, and the distribution of ion density surrounding the probe. This study lays the basis for such a model, which will incorporate measurement of ion velocity distribution and other parameters not fully captured in this work. The development of this new model represents a significant challenge and a future research direction.

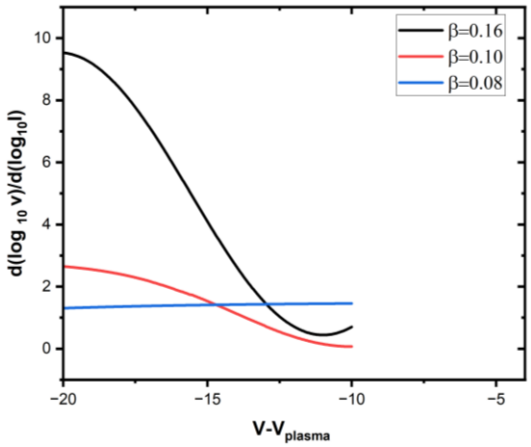

Fig. (5) d($\log_{10}$(V)/d($\log_{10}$(I)) curves for Ar-N_2 plasma RF magnetron experimental data from cylindrical Langmuir probe at values of β= 0.08, 0.1, and 0.16

4. Conclusion

This study investigates positive ion motion in Ar-N_2 RF plasma using four criteria. The ABR model accurately predicted the experimental results for the first and second criteria. The OML model agreed with the third and fourth criteria. Although this agreement was limited for the fourth criterion at high β values. The results suggest neither the OML nor ABR models fully describe ion behavior under all conditions. The ABR model shows good agreement for β=0.08 and 0.1, deviations occur at β=0.16 in an RF Ar-N_2 plasma, while the OML model shows better agreement for at β=0.16 values.

References

[1] D. Darian et al., "Theory and simulation of spherical and cylindrical Langmuir probe in non-Maxwellian plasmas", *Plasma Phys. Control. Fusion*, 61(8) (2019) 085025.

[2] F. Chen, "Langmuir probe measurement in the intense RF field of a helicon discharge", *Plasma Sources Sci. Technol*, 21(5) (2012) 055013.

[3] K. Kjlerbakken, J. Miloch and K. Røed, "Sheath formation time for spherical Langmuir probes", *J. Plasma Phys.,* 89(1) (2023) 905890102.

[4] A. Aghaei et al., "Effect of deposition rate on anti-refection and wettability properties of RF magnetron sputtering SiCON thin film", *Opt. Quantum Electron.,* 56(92) (2024) 1-17.

[5] C. Chulhee et al., "Determination of Plasma Potential Using an Emissive Probe with Floating Potential Method", *Materials*, 16(7) (2023) 2762.

[6] B. Robert, and E. Brain, "Recommended Practice for Use of Langmuir Probes in Electric Propulsion Testing", *J. Propul. Power*, 33(3) (2017) 1-25.

[7] F. Chen, "Langmuir probe analysis for high-density plasma", *Phys. Plasmas*, 8(6) (2001) 3029 -3041.

[8] A. Metawa et al., "Langmuir probe and optical emission spectroscopy studies for RF magnetron sputtering during TiON thin film deposition", *Chinese J. Phys.*, 68 (2020) 168–17.

[9] H. Richard, and L. Stanley, **"Plasma Diagnostics Techniques"**, Academic Press (NY, 1965), p. 406.

[10] M. Leberman and A. Lichtenberg, **"Principles of Plasma Discharges and Materials Processes"**, John-Wiley & Sons (2005), p. 445.

[11] K. An et al., "Two-step fabrication of thin film encapsulation using laser-assisted chemical vapor deposition and laser-assisted plasma enhanced chemical vapor deposition for long-lifetime organic light-emitting diodes", *Org. Electron.*, 91 (2021) 106078.

[12] E. Shaaban et al., "Investigation of structural and optical properties of near-surface of CdTe film induced by nitrogen plasma immersion ion implantation", *Mater. Res. Exp.*, 5(8) (2018) 086402.

[13] A. Mahmoud et al., "Comparisons of atomic layer etching of silicon in Cl_2 and HBr-containing plasmas", *J. Vac. Sci. Technol A*., 43(1) (2025) 012601.

[14] X Zhao et al., "The Effect of In Situ Laser-Assisted Plasma Spraying on the Plasma Etching Resistance of Yttrium Oxide Coating", *Coatings*, 14(11) (2024) 1427.

[15] W. Wang et al., "Influence of Annealing Temperature on the Properties of $ZnGa_2O_4$ Thin Films by Magnetron Sputtering", *Coatings*, 9(12) (2019) 859.

[16] P. Moura, and S. Serio, "Recent Applications and Future Trends of Nanostructured Thin Films-Based Gas Sensors Produced by Magnetron Sputtering", *Coatings*, 14(9) (2024) 1214.

[17] A. Shamima, et al., "RF sputtered GZO thin films for enhancing electrons transport in perovskite solar cells", *Opt. Mater.*, 149 (2024) 115006.

[18] D. Voloshin et al., "Evaluation of plasma density in RF CCP discharges from ion current to Langmuir probe: experiment and numerical simulation", *Eur. Phys. J. D*, 69(23) (2015) 1-9.

[19] F. Guillermo et al., "Influence of collisions in a fluid model for the warm-ion sheath around a cylindrical Langmuir probe", *Plasma Sourc. Sci. Technol.*, 28(11) (2019) 115017.

[20] F. José et al., "Theoretical ion current to cylindrical Langmuir probes for finite ion temperature values", *J. Phys. D Appl. Phys.*, 29(11) (1996) 2832–2840.

[21] R. Crespo et al., "Analytical fit of the I-V characteristic for cylindrical and spherical Langmuir probe in electronegative plasmas", *J. Appl. Phys*., 96(9) (2004) 4777–4783.

[22] M. Juan et al., "Accurate measurement of the ion saturation current collected by a cylindrical Langmuir

probe in cold plasmas", *Plasma Process Polym*., 17(11) (2020) e2000073.
[23] A. Pedro and M. Richard, "Simulation Inference of Plasma Parameters from Langmuir Probe Measurements", *Earth Space Sci.*, 18(3) (2021) EA001344.
[24] K. Yasserian and M. Aslaninejad, "Edge of magnetized electronegative plasma ion source in the presence of collisional adiabatic thermal positive ions", *J. Theor. Appl. Phys.*, 13(3) (2019) 251–261.
[25] G. Regodón et al., "Influence of the Ion Mass in the Radial to Orbital Transition in Weakly Collisional Low-Pressure Plasmas Using Cylindrical Langmuir Probes", *Appl. Sci*., 10(17) (2020) 5727.
[26] V. Riaby et al., "RF plasma probe diagnostics: a method for eliminating measurement errors for Langmuir probes with bare protective shields", *IOP J. Phys.: Conf. Ser.*, 958 (2018) 012006.
[27] V. Riaby et al., "Method for reducing measurement errors Langmuir probe with protective RF shielding", *J. Appl. Phys*., 123(16) (2018) 163301.
[28] F. Chen, "Langmuir probe in RF plasma surprising validity of OML theory", *Plasma Sourc. Phys. Plasmas*, 18(3) (2009) 035012.
[29] X. Chen and G. Sanchez-Arriaga, "Orbital Motion theory and Operation Regimes for cylindrical emissive probe", *Phys. Plasmas*, 24(2) (2017) 023504.
[29] F. Chen, "Langmuir probe measurement in the intense RF field of a helicon discharge", *Plasma Sourc. Sci. Technol.*, 21(5) (2012) 055013.
[30] Z. Petr et al., "Particle-in-cell/Monte Carlo simulation of electron and ion currents to cylindrical Langmuir probe", *Contrib. Plasma Phys*., 59(3) (2018) 314-325.
[31] A. Howling, P. Guittienne and I. Furno, "Two-fluid plasma model for radial Langmuir probes as a converging nozzle with sonic choked flow, and sonic passage to supersonic flow", *Phys. Plasmas*, 26(4) (2019) 044502.
[32] H. Ghomi et al., "Plasma sheath criterion in thermal electronegative plasmas", *J. Appl. Phys*., 108(6) (2010) 063302.
[33] B. Vincent et al., "Electron properties of an emissive cathode: analysis with incoherent Thomson scattering. fluid simulations and Langmuir probe measurements", *J. Phys. D: Appl. Phys*., 53(41) (2020) 415202.
[34] T. David et al., "PIC/MCC Simulation of Electron and Ion Currents to Spherical Langmuir Probe", *Contrib. Plasma Phys*., 55(6) (2015) 481-493.
[35] P. Bryant, "Theory of cylindrical Langmuir probes in weakly ionized, non-thermal, stationary and moderately collisional plasmas", *Plasma Sourc. Sci. Technol*., 18(1) (2009) 014013.
[36] F. Chen, **"Plasma Diagnostic Techniques"**, Ch. 5, Academic Press (NY, 196).
[37] E. Allen, "Probe theory - the orbital motion approach", *Physica Scripta*, 45(5) (1992) 497-503.
[38] A. Sonin, "The free molecule Langmuir probe and its use in flow field studies", *AIAA J.*, 4(9) (1966) 1588.
[39] E. Allen, "Probe theories and applications: modern aspects", *Plasma Sourc. Sci. Technol.*, 4(2) (1995) 234-241.
[40] J. Laframboise, "Theory of cylindrical probe in collisionless of magnetoplasma", *Phys. Fluids*, 19(12) (1976) 1900-1908.
[41] E. Peterson and L. Talbot, "Langmuir probe response in a turbulent plasma", *AIAA J.*, 8(8) (1970) 1391.
[42] E. Allen, J. Boyd and P. Reynolds, "The Collection of Positive Ions by a Probe Immersed in a Plasma", *Proc. Phys. Soc. B.*, 70(3) (1957) 297–304.
[43] J. Chun-Sung, J. Wojciech and M. Yohei, "Collected Current by a Double Langmuir Probe Setup with Plasma Flow", *IEEE Trans. Plasma Sci.*, 52(10) (2024) 5222-5233.
[44] L. Pilling and D. Carnegie, "Validating experimental and theoretical Langmuir probe analyses", *Plasma Sourc. Sci. Technol.*, 16(3) (2007) 570.

Table (1) Comparison between the criteria and applicability of them to OML or ABR models

Criterion	Applicability OML/ABR	Advantages	Disadvantages
Comparison of the experimental (I-V curve) and theoretical curves (OML and ARB models) in the ion saturation region	**-ABR model (**Applicable) -OML model (Not applicable)	-Applicable to a wide range of ion saturation in I-V curves - Its insensitivity to noise	-It is independent of the β values
(Sonin plot)	**-ABR model** Applicable at (β = 0.08 and β = 0.10) -OML model (Not applicable)	-This criterion applicability depends on the β values -It offers helpful diagnostic techniques for positive ions	-Noise influences the criterion -This criterion utilizes a single point data point (current) from the experimental I-V curve - It's high sensitivity to the β values
(I^2-V) curve	**-ABR model** (Not applicable) -**OML model** Applicable in Ar/N_2 at (70% and 60 % Ar)	-It used a wide range of I-V curves	- The linearity of the curve affects the level of noise in the data. - It ensures orbital or non-orbital motion for ions
(Pilling-Carnegie)	**-ABR model** (Not applicable) -**OML model** Applicable at (β = 0.08 and β = 0.10)	-It depends on the values β -It used a wide range of I-V curves	-The experimental noise effect on the logarithm of the voltage and current makes it difficult to arrive at the limiting value of 2 -It determines whether ions undergo orbital or non-orbital motion, but provides no information about their radial behavior

